

Electronic Supplementary Information

**Zeolite-Like Ion-Exchanged Cu-Attapulgite Catalysts  
for Promoted Selective Oxidation of Ammonia**

Xuebin Zhang, Tianwei Lan, Qiuying Yi, Yufei Wang, Danhong Cheng\* and  
Dengsong Zhang\*

*International Joint Laboratory of Catalytic Chemistry, State Key Laboratory of  
Advanced Special Steel, Innovation Institute of Carbon Neutrality, Department of  
Chemistry, College of Sciences, Shanghai University, Shanghai 200444, China.*

*\*To whom correspondence should be addressed.*

E-mail: [dszhang@shu.edu.cn](mailto:dszhang@shu.edu.cn) (DS Zhang); [cdh@shu.edu.cn](mailto:cdh@shu.edu.cn) (DH Cheng).

## Table of Contents

|  |    |
|--|----|
| <b>Additional materials and methods</b> .....  | 6  |
| <b>NH<sub>3</sub> oxidation measurements</b> .....   | 8  |
| <b>Catalyst Characterization</b> .....   | 9  |
| <b>Fig. S1.</b> Plots of NH <sub>3</sub> conversion (solid lines) and N <sub>2</sub> selectivity (dash lines) versus temperature over Cu-ATP-WIE and Cu-ATP-SSIE catalysts. Reaction conditions: 500 ppm NH <sub>3</sub> , 5 vol % O <sub>2</sub> balanced with N <sub>2</sub> , and 80,000 h <sup>-1</sup> of GHSV. ....                          | 11 |
| <b>Fig. S2.</b> Plots of NH <sub>3</sub> conversion (solid lines) and N <sub>2</sub> selectivity (dash lines) versus temperature over Cu-ATP-60-3 and Cu-ATP-90-3 catalysts. Reaction conditions: 500 ppm NH <sub>3</sub> , 5 vol % O <sub>2</sub> balanced with N <sub>2</sub> , and 80,000 h <sup>-1</sup> of GHSV. ....                         | 12 |
| <b>Fig. S3.</b> Plots of NH <sub>3</sub> conversion (solid lines) and N <sub>2</sub> selectivity (dash lines) versus temperature over Cu-ATP-90-1.5, Cu-ATP-90-3 and Cu-ATP-90-4.5 catalysts. Reaction conditions: 500 ppm NH <sub>3</sub> , 5 vol % O <sub>2</sub> balanced with N <sub>2</sub> , and 80,000 h <sup>-1</sup> of GHSV.....         | 13 |
| <b>Fig. S4.</b> Plots of NH <sub>3</sub> conversion (solid lines) and N <sub>2</sub> selectivity (dash lines) versus temperature over Cu-ATP-500-1 and Cu-ATP-BM-500-1 catalysts. Reaction conditions: 500 ppm NH <sub>3</sub> , 5 vol % O <sub>2</sub> balanced with N <sub>2</sub> , and 80,000 h <sup>-1</sup> of GHSV...                       | 14 |
| <b>Fig. S5.</b> Plots of NH <sub>3</sub> conversion (solid lines) and N <sub>2</sub> selectivity (dash lines) versus temperature over Cu-ATP-BM-500-1, Cu-ATP-BM-500-2 and Cu-ATP-BM-500-3 catalysts. Reaction conditions: 500 ppm NH <sub>3</sub> , 5 vol % O <sub>2</sub> balanced with N <sub>2</sub> , and 80,000 h <sup>-1</sup> of GHSV..... | 15 |
| <b>Fig. S6.</b> Plots of NH <sub>3</sub> conversion (solid lines) and N <sub>2</sub> selectivity (dash lines) versus   |    |

|  |    |
|--|----|
| temperature over Cu-ATP-BM-500-1, Cu-ATP-BM-400-1 and Cu-ATP-BM-300-1 catalysts. Reaction conditions: 500 ppm NH <sub>3</sub> , 5 vol % O <sub>2</sub> balanced with N <sub>2</sub> , and 80,000 h <sup>-1</sup> of GHSV.....  | 16 |
| <b>Fig. S7.</b> Plots of NH <sub>3</sub> conversion (solid lines) and N <sub>2</sub> selectivity (dash lines) versus temperature over ATP support. Reaction conditions: 500 ppm NH <sub>3</sub> , 5 vol % O <sub>2</sub> balanced with N <sub>2</sub> , and 80,000 h <sup>-1</sup> of GHSV. ....   | 17 |
| <b>Fig. S8.</b> Plots of N-containing products selectivity versus temperature over the Cu-ATP catalyst. Reaction conditions: 500 ppm NH <sub>3</sub> , 5 vol % O <sub>2</sub> balanced with N <sub>2</sub> , and 50,000 h <sup>-1</sup> of GHSV.....   | 18 |
| <b>Fig. S9.</b> Plots of N-containing products selectivity versus temperature over the CuO/ATP catalyst. Reaction conditions: 500 ppm NH <sub>3</sub> , 5 vol % O <sub>2</sub> balanced with N <sub>2</sub> , and 50,000 h <sup>-1</sup> of GHSV.....  | 19 |
| <b>Fig. S10.</b> Plots of NH <sub>3</sub> conversion (solid lines) and N <sub>2</sub> selectivity (dash lines) versus temperature over the Cu-ATP catalyst. Reaction conditions: 500 ppm NH <sub>3</sub> , 5 vol % O <sub>2</sub> balanced with N <sub>2</sub> , and 50,000 h <sup>-1</sup> of GHSV. ....  | 20 |
| <b>Fig. S11.</b> Plots of NH <sub>3</sub> conversion (solid lines) and N <sub>2</sub> selectivity (dash lines) as a function of time on stream in the presence of H <sub>2</sub> O at 330 °C for Cu-ATP catalyst. Reaction conditions: 500 ppm NH <sub>3</sub> , 5 vol % O <sub>2</sub> , 3 vol% H <sub>2</sub> O balanced with N <sub>2</sub> , and 50,000 h <sup>-1</sup> of GHSV..... | 21 |
| <b>Fig. S12.</b> Plots of NH <sub>3</sub> conversion (solid lines) and N <sub>2</sub> selectivity (dash lines) versus temperature over Cu-ATP and Cu-SSZ-13 catalysts. Reaction conditions: 500 ppm NH <sub>3</sub> , 5 vol % O <sub>2</sub> balanced with N <sub>2</sub> , and 50,000 h <sup>-1</sup> -150,000 h <sup>-1</sup> of GHSV. ....  | 22 |

|   |    |
|---|----|
| <b>Fig. S13.</b> Plots of NH <sub>3</sub> conversion (solid lines) and N <sub>2</sub> selectivity (dash lines) versus temperature over the Cu-MMT catalyst. Reaction conditions: 500 ppm NH <sub>3</sub> , 5 vol % O <sub>2</sub> balanced with N <sub>2</sub> , and 50,000 h <sup>-1</sup> of GHSV. .... | 23 |
| <b>Fig. S14.</b> SEM image of ATP support. ....   | 24 |
| <b>Fig. S15.</b> (A) SEM image; (B) EDS mapping results of overlapped image and (B <sub>1</sub> ) Cu, (B <sub>2</sub> ) Si, (B <sub>3</sub> ) O, (B <sub>4</sub> ) Al, and (B <sub>5</sub> ) Mg elements distribution over the Cu-ATP catalyst. ....  | 25 |
| <b>Fig. S16.</b> (A) SEM image; (B) EDS mapping results of overlapped image and (B <sub>1</sub> ) Cu, (B <sub>2</sub> ) Si, (B <sub>3</sub> ) O, (B <sub>4</sub> ) Al, and (B <sub>5</sub> ) Mg elements distribution over the CuO/ATP catalyst. ....   | 26 |
| <b>Fig. S17.</b> (A)TEM image; (A <sub>1</sub> ) EDS mapping results of overlapped image and (A <sub>2</sub> ) Cu elements distribution over the Cu-ATP; (B) TEM image; (B <sub>1</sub> ) EDS mapping results of overlapped image and (B <sub>2</sub> ) Cu elements distribution over the CuO/ATP. ....   | 27 |
| <b>Fig. S18.</b> (A) EDS mapping results of overlapped image and (A <sub>1</sub> ) O, (A <sub>2</sub> ) Si, (A <sub>3</sub> ) Al, (A <sub>4</sub> ) Mg elements distribution over the Cu-ATP catalyst. ....   | 28 |
| <b>Fig. S19.</b> (A) EDS mapping results of overlapped image and (A <sub>1</sub> ) O, (A <sub>2</sub> ) Si, (A <sub>3</sub> ) Al, (A <sub>4</sub> ) Mg elements distribution over the CuO/ATP catalyst. ....  | 29 |
| <b>Fig. S20.</b> The line scanning image of TEM-energy dispersive X-ray spectroscopy (EDS) over the CuO/ATP catalyst. ....  | 30 |
| <b>Fig. S21.</b> N <sub>2</sub> physisorption isotherms of ATP support, ATP-BM, Cu-ATP, CuO/ATP and CuO/ATP-BM catalysts. ....  | 31 |
| <b>Fig. S22.</b> O 1s XPS spectra for Cu-ATP and CuO/ATP catalysts. ....  | 32 |

|   |    |
|---|----|
| <b>Fig. S23.</b> H <sub>2</sub> -TPR profiles for Cu-ATP, CuO/ATP catalysts and ATP support. ....   | 33 |
| <b>Fig. S24.</b> Py-IR spectra for the Cu-ATP catalyst. ....  | 34 |
| <b>Fig. S25.</b> Py-IR spectra for the CuO/ATP catalyst. ....   | 35 |
| <b>Fig. S26.</b> Py-IR spectra for the ATP support. ....  | 36 |
| <b>Fig. S27.</b> The NH <sub>3</sub> adsorption spectra of ATP support.....   | 37 |
| <b>Fig. S28.</b> The N <sub>2</sub> signal detected by mass spectrometry of Cu-ATP and CuO/ATP catalysts. ....  | 38 |
| <b>Table S1.</b> Cu element content of Cu-ATP, CuO/ATP, Cu-SSZ-13, Cu-ZSM-5 and Cu-SAPO-34 catalysts. ....  | 39 |
| <b>Table S2.</b> The specific surface area, pore volume and pore size information obtained from the N <sub>2</sub> adsorption-desorption isotherms analysis of ATP support, ATP-BM, Cu-ATP, CuO/ATP and CuO/ATP-BM catalysts..... | 40 |
| <b>References</b> .....   | 41 |

## Additional materials and methods

Attapulgite was provided by Shijiazhuang Yuxin Building Materials Co., Ltd, the ammonium chloride and copper nitrate trihydrate was purchased from Sinopharm Chemical Reagent Co. Ltd (China). All the reagents were used without further purification.

The Cu-ATP-WIE was prepared by a two-step ion-exchange method. First, an appropriate amount of  $\text{NH}_4\text{Cl}$  was used as the ammonium-ion exchange precursor reacting with ATP for 2 h at 80 °C to obtain the  $\text{NH}_4^+$ -ATP. Then,  $\text{NH}_4^+$ -ATP was reacted with  $0.05 \text{ mol}\cdot\text{L}^{-1} \text{ Cu}(\text{NO}_3)_2\cdot 3\text{H}_2\text{O}$  at 90 °C for 3 h to achieve the  $\text{Cu}^{2+}$  exchange. The product was washed with deionized water and collected by centrifugation. After drying overnight at 80 °C, the obtained powdery sample was calcined at 500 °C for 2 h. The sample obtained by  $\text{Cu}^{2+}$  exchange was named Cu-ATP-WIE. In this step, the sample prepared by changing the oil bath temperature and time was named Cu-ATP-A-B, where A was the oil bath temperature (°C) and B was oil bath time (h).

The Cu-ATP-SSIE was synthesized by solid-state ion exchange method. First, dissolve 0.2353 g  $\text{Cu}(\text{NO}_3)_2\cdot\text{H}_2\text{O}$  in 3 mL ethanol and stir well. Then add 2 g ATP powder slowly, seal and stir for 15 min. Perforated to breathable, leave at room temperature for 1.5 days. After full grinding, the calcination condition was 550 °C for 4 h.

The Cu-SSZ-13 catalyst was prepared by direct calcination of commercial Cu-SSZ-13 catalyst. The synthesis method of Cu-MMT catalyst was consistent with that

of Cu-ATP catalyst.

Cu-MMT was prepared by a two-step ion-exchange method. First, MMT was pretreated by ball milling (MMT-BM). An appropriate amount of  $\text{NH}_4\text{Cl}$  was used as the ammonium-ion exchange precursor reacting with MMT-BM for 2 h at 80 °C to obtain the  $\text{NH}_4^+$ -MMT-BM. Then,  $\text{NH}_4^+$ -MMT-BM was reacted with  $0.05 \text{ mol}\cdot\text{L}^{-1}$   $\text{Cu}(\text{NO}_3)_2\cdot 3\text{H}_2\text{O}$  at 90 °C for 3 h to achieve the  $\text{Cu}^{2+}$  exchange. The product was washed with deionized water and collected by centrifugation. This procedure was repeated two times. After drying overnight at 80 °C, the obtained powdery sample was calcined at 400 °C for 2 h.

### **NH<sub>3</sub> oxidation measurements**

The reaction rate was calculated by the equation:

$$r = \frac{V \times ([NH_3]_{inlet} - [NH_3]_{outlet})}{V_m \times 10000 \times M_{cat}}$$

Where V is the velocity of the gas (L·s<sup>-1</sup>), [NH<sub>3</sub>] is the concentration of NH<sub>3</sub> (ppm), V<sub>m</sub> is the volume of 1 mole of an ideal gas (L), M<sub>cat</sub> is the weight of the catalysts (g).

## Catalyst Characterization

The Cu element contents of the samples were determined by ICP-OES (Agilent 5110). Power X-ray diffraction (XRD) measurements were conducted on a Bruker D8 Advance diffractometer equipped with a Cu K $\alpha$  radiation source over a  $2\theta$  range of 10–70°. Electron paramagnetic resonance (EPR) spectra were recorded on JES X320 at a temperature of -196 °C. High resolution transmission electron microscopy (HRTEM) images were collected by a JEOL JEM2100F field-emission electron microscopy at 200 kV. The N<sub>2</sub> adsorption-desorption analysis of the samples was performed at 77 K using a U.S. Quanta chrome ASAP 2020M nitrogen adsorption instrument. UV–vis diffuse reflectance (DR-UV–vis) spectra were performed by a UV–vis spectrophotometer (Cary5000, Agilent, USA) and using BaSO<sub>4</sub> as a reference. X-ray photoelectron spectroscopy (XPS) was performed using PHI-5300 electron spectrometer of Mg K $\alpha$  radiation. H<sub>2</sub> temperature programmed reduction (H<sub>2</sub>-TPR) was performed using a Micrometrics AutoChem 2950 instrument under 10% H<sub>2</sub>/Ar gas flow (TCD). A series of temperature-programmed experiments including NH<sub>3</sub>-TPD and NH<sub>3</sub>-O<sub>2</sub>-TPSR were operated on a Micrometrics AutoChem 2920 instrument coupled with a MS (Pfeiffer Vacuum GSD 320). In NH<sub>3</sub>-TPD, all samples (80 mg) were pretreated in He at 300 °C in a quartz reactor for 30 min, and then 30 mL·min<sup>-1</sup> 10% NH<sub>3</sub>/He gas flow was introduced at 100 °C for 60 min for the NH<sub>3</sub> adsorption. After that, He was introduced to purge the physisorbed NH<sub>3</sub> and stabled the baseline. Chemisorption profiles and MS signals were collected from 100 °C to 800 °C. In NH<sub>3</sub>-O<sub>2</sub>-TPSR, all catalysts (80 mg) were pretreated in He at

300 °C for 30 min, and 30 mL·min<sup>-1</sup> 10% NH<sub>3</sub>/He gas flow was introduced for NH<sub>3</sub> adsorption at 100 °C. After being purged by He for 30 min, 30 mL·min<sup>-1</sup> 2% O<sub>2</sub>/He gas flow was introduced and MS signals were recorded from 100 °C to 700 °C. Pyridine-IR spectra of all samples were collected on a Nicolet 6700 spectrometer equipped with an MCT detector. All samples were pre-treated in 30 mL·min<sup>-1</sup> He at 300 °C for 30 min and background files were collected at different temperature. As for *in situ* DRIFTS recorded during NH<sub>3</sub> desorption and NH<sub>3</sub> surface reaction experiments, 1000 ppm NH<sub>3</sub> in 30 mL/min NH<sub>3</sub>/He gas was introduced at 50 °C for 60 min, the spectra were collected at different temperatures. For *in situ* DRIFTS recorded during NH<sub>3</sub> + O<sub>2</sub> surface reaction experiments, 30 mL·min<sup>-1</sup> gas flow containing 1000 ppm NH<sub>3</sub> and 5% O<sub>2</sub> was introduced into the reactor and the spectra at different temperature were collected. For *in situ* DRIFTS recorded in O<sub>2</sub> pulsed in continuous NH<sub>3</sub> flow, all samples were pre-treated in 30 mL·min<sup>-1</sup> He at 300 °C for 30 min and background files were collected at 200 °C. After that, 30 mL·min<sup>-1</sup> gas flow containing 1000 ppm NH<sub>3</sub> was continuously introduced for 30 min. And then, 5% O<sub>2</sub>/He was injected for 5 min and stopped or 5 min, which was repeated for 3 times. The composition of the tail gas was monitored by MS.

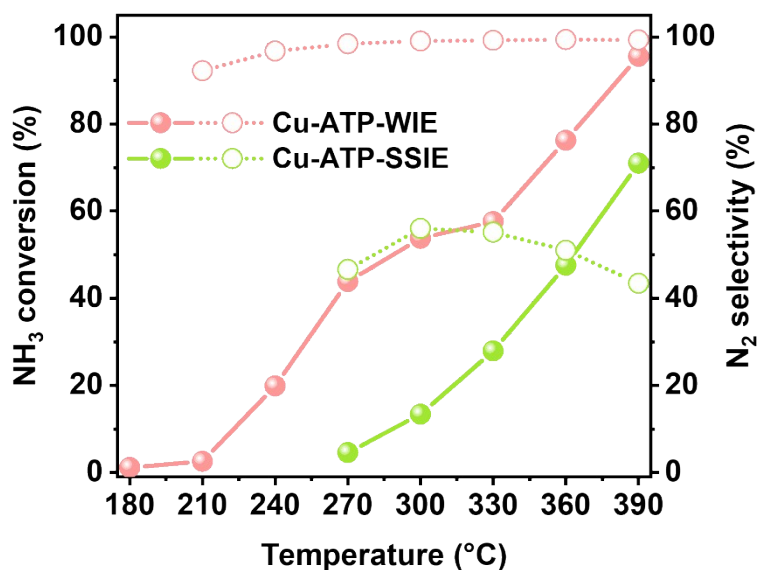


**Fig. S1.** Plots of NH<sub>3</sub> conversion (solid lines) and N<sub>2</sub> selectivity (dash lines) versus temperature over Cu-ATP-WIE and Cu-ATP-SSIE catalysts. Reaction conditions: 500 ppm NH<sub>3</sub>, 5 vol % O<sub>2</sub> balanced with N<sub>2</sub>, and 80,000 h<sup>-1</sup> of GHSV.

The NH<sub>3</sub>-SCO performance of Cu-ATP-WIE catalyst which synthesized by a wet ion exchange method (WIE) was better and N<sub>2</sub> selectivity was close to 100%. The Cu-ATP-SSIE catalyst synthesized by a solid-state ion exchange method (SSIE) might contain a lot of CuO.

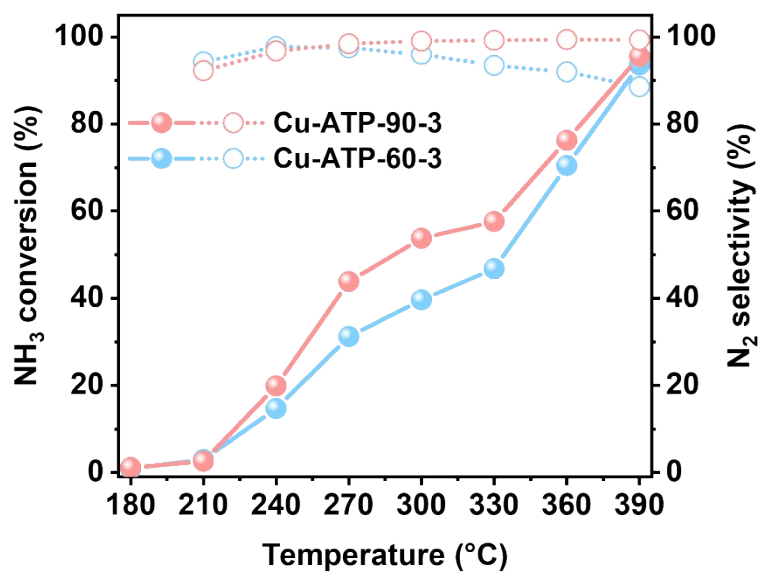


**Fig. S2.** Plots of NH<sub>3</sub> conversion (solid lines) and N<sub>2</sub> selectivity (dash lines) versus temperature over Cu-ATP-60-3 and Cu-ATP-90-3 catalysts. Reaction conditions: 500 ppm NH<sub>3</sub>, 5 vol % O<sub>2</sub> balanced with N<sub>2</sub>, and 80,000 h<sup>-1</sup> of GHSV.

The catalyst optimization in Fig. S2, S3 only changed the oil bath temperature and time. It was better to use 90 °C as oil bath temperature for copper exchange.

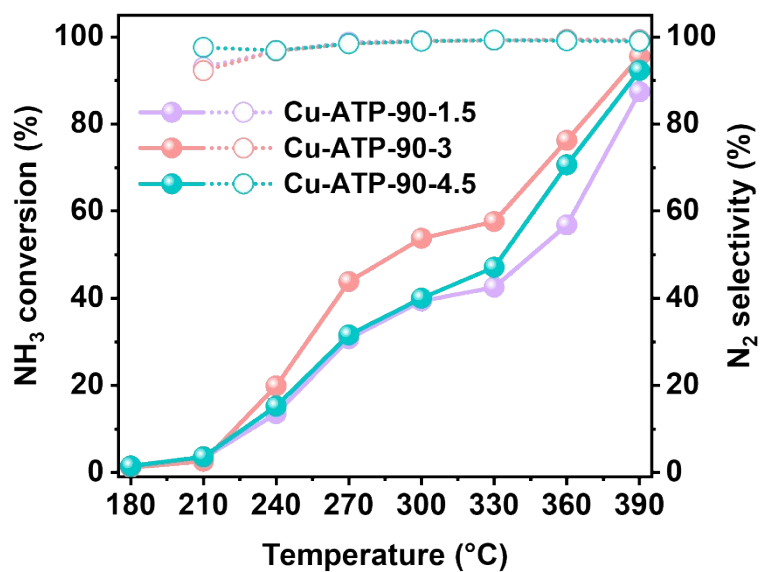


**Fig. S3.** Plots of NH<sub>3</sub> conversion (solid lines) and N<sub>2</sub> selectivity (dash lines) versus temperature over Cu-ATP-90-1.5, Cu-ATP-90-3 and Cu-ATP-90-4.5 catalysts. Reaction conditions: 500 ppm NH<sub>3</sub>, 5 vol % O<sub>2</sub> balanced with N<sub>2</sub>, and 80,000 h<sup>-1</sup> of GHSV.

It was better to use 3 h as oil bath time for copper exchange.

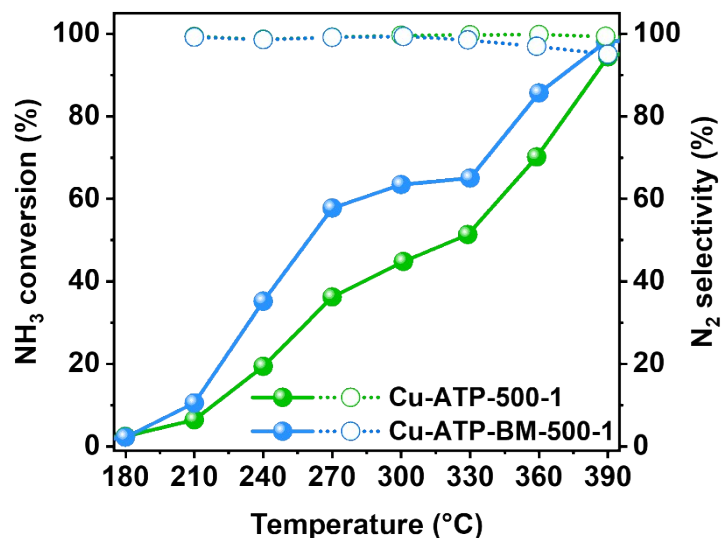


**Fig. S4.** Plots of NH<sub>3</sub> conversion (solid lines) and N<sub>2</sub> selectivity (dash lines) versus temperature over Cu-ATP-500-1 and Cu-ATP-BM-500-1 catalysts. Reaction conditions: 500 ppm NH<sub>3</sub>, 5 vol % O<sub>2</sub> balanced with N<sub>2</sub>, and 80,000 h<sup>-1</sup> of GHSV.

The synthetic oil bath temperature of the subsequent samples was fixed at 90°C and the time was fixed at 3h, and the name was not repeat marked. The catalytic performance of Cu-ATP-BM-500-1 catalyst was better than Cu-ATP-500-1 catalyst without ball milling treatment. It could be speculated that the specific surface area of ATP increased after ball milling, which prompted more Cu<sup>2+</sup> exchanged into the support.

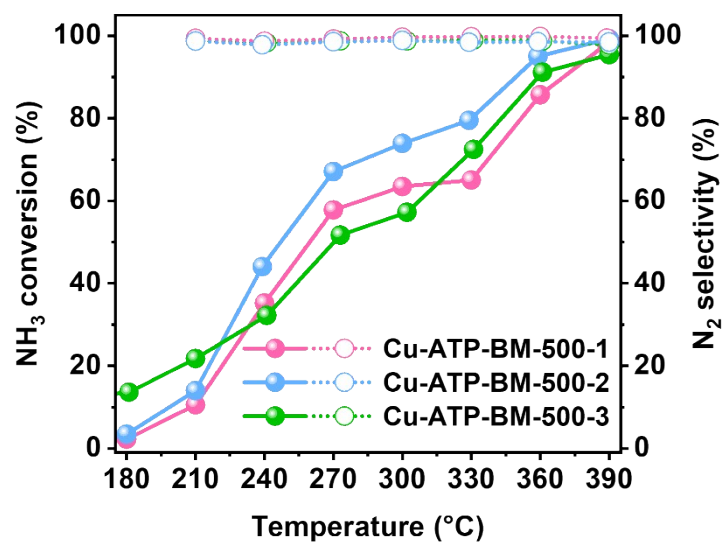


**Fig. S5.** Plots of NH<sub>3</sub> conversion (solid lines) and N<sub>2</sub> selectivity (dash lines) versus temperature over Cu-ATP-BM-500-1, Cu-ATP-BM-500-2 and Cu-ATP-BM-500-3 catalysts. Reaction conditions: 500 ppm NH<sub>3</sub>, 5 vol % O<sub>2</sub> balanced with N<sub>2</sub>, and 80,000 h<sup>-1</sup> of GHSV.

Increasing times of ion-exchange could improve the catalytic performance to a certain extent because of the full exchange of Cu<sup>2+</sup>.

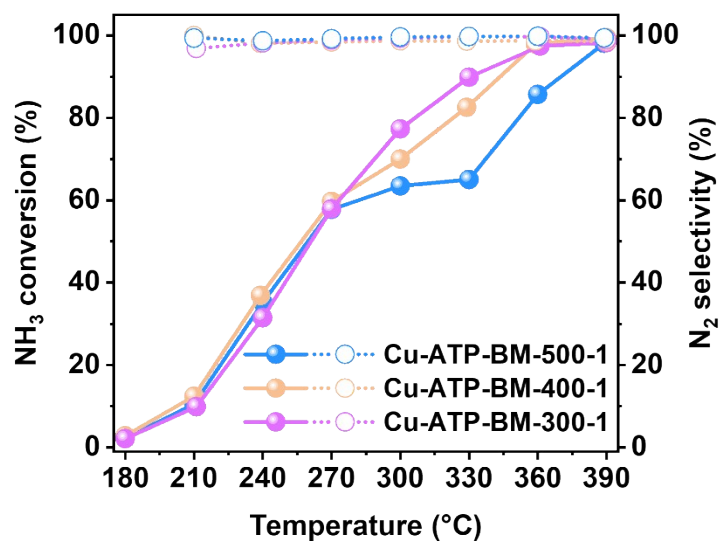


**Fig. S6.** Plots of NH<sub>3</sub> conversion (solid lines) and N<sub>2</sub> selectivity (dash lines) versus temperature over Cu-ATP-BM-500-1, Cu-ATP-BM-400-1 and Cu-ATP-BM-300-1 catalysts. Reaction conditions: 500 ppm NH<sub>3</sub>, 5 vol % O<sub>2</sub> balanced with N<sub>2</sub>, and 80,000 h<sup>-1</sup> of GHSV.

Changing the calcination temperature would also cause some effects. The best calcination temperature was 400 °C. It was indicated that the catalyst which carry out two ion-exchange processes after ball milling pretreatment, and calcined at 400 °C for 2 h, possessed high catalytic performance.

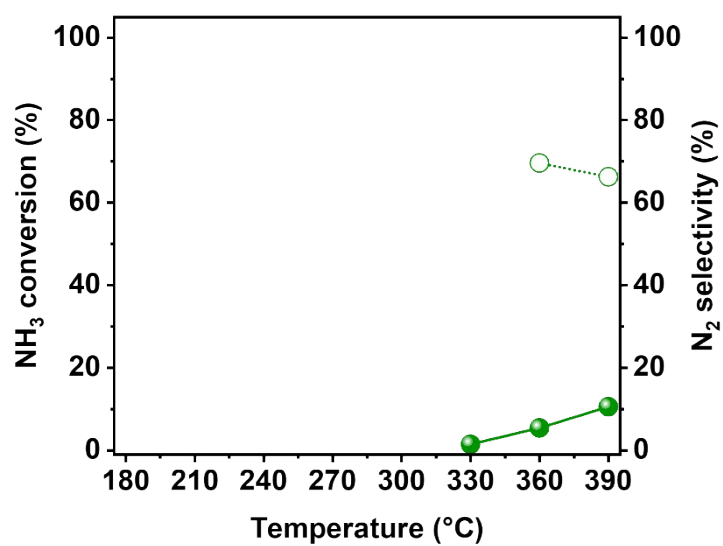


**Fig. S7.** Plots of NH<sub>3</sub> conversion (solid lines) and N<sub>2</sub> selectivity (dash lines) versus temperature over ATP support. Reaction conditions: 500 ppm NH<sub>3</sub>, 5 vol % O<sub>2</sub> balanced with N<sub>2</sub>, and 80,000 h<sup>-1</sup> of GHSV.

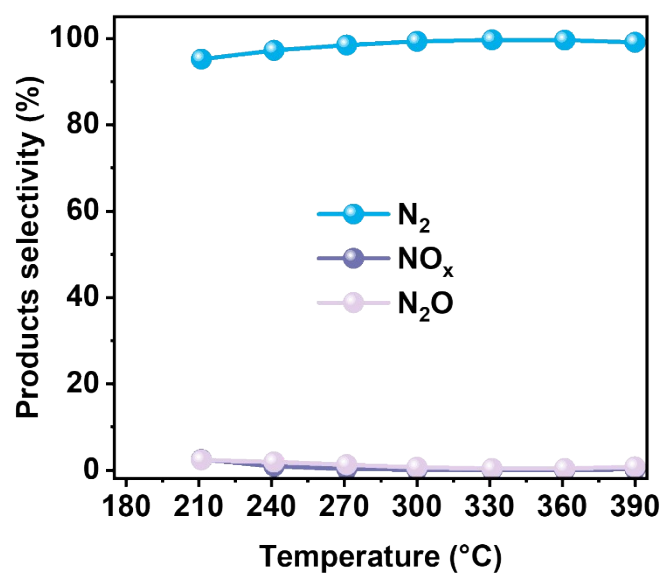


**Fig. S8.** Plots of N-containing products selectivity versus temperature over the Cu-ATP catalyst. Reaction conditions: 500 ppm NH<sub>3</sub>, 5 vol % O<sub>2</sub> balanced with N<sub>2</sub>, and 50,000 h<sup>-1</sup> of GHSV.

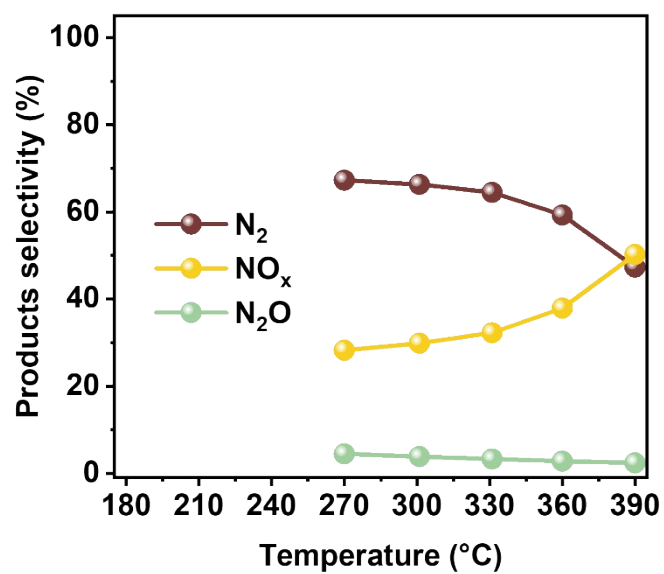


**Fig. S9.** Plots of N-containing products selectivity versus temperature over the CuO/ATP catalyst. Reaction conditions: 500 ppm NH<sub>3</sub>, 5 vol % O<sub>2</sub> balanced with N<sub>2</sub>, and 50,000 h<sup>-1</sup> of GHSV.

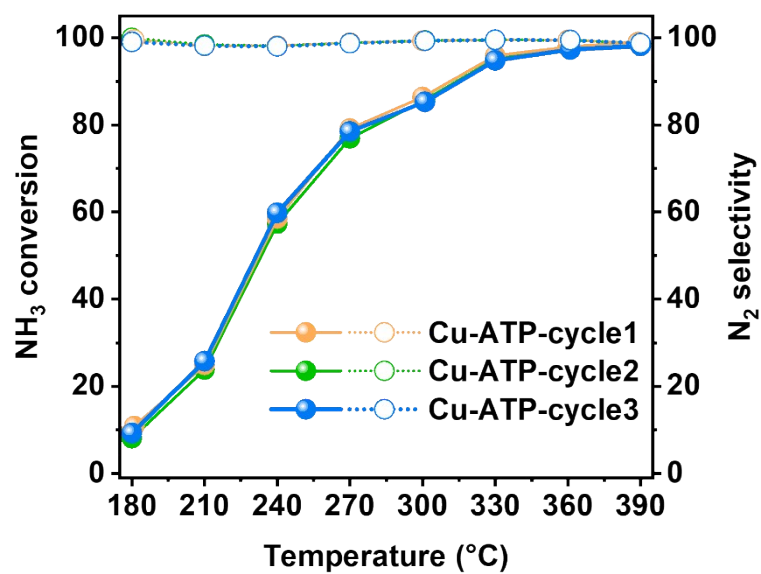


**Fig. S10.** Plots of NH<sub>3</sub> conversion (solid lines) and N<sub>2</sub> selectivity (dash lines) versus temperature over the Cu-ATP catalyst. Reaction conditions: 500 ppm NH<sub>3</sub>, 5 vol % O<sub>2</sub> balanced with N<sub>2</sub>, and 50,000 h<sup>-1</sup> of GHSV.

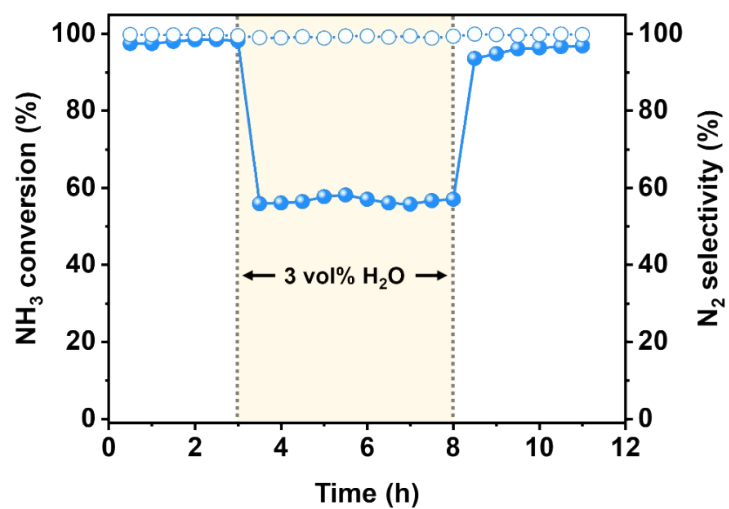


**Fig. S11.** Plots of NH<sub>3</sub> conversion (solid lines) and N<sub>2</sub> selectivity (dash lines) as a function of time on stream in the presence of H<sub>2</sub>O at 330 °C for Cu-ATP catalyst. Reaction conditions: 500 ppm NH<sub>3</sub>, 5 vol % O<sub>2</sub>, 3 vol% H<sub>2</sub>O balanced with N<sub>2</sub>, and 50,000 h<sup>-1</sup> of GHSV.

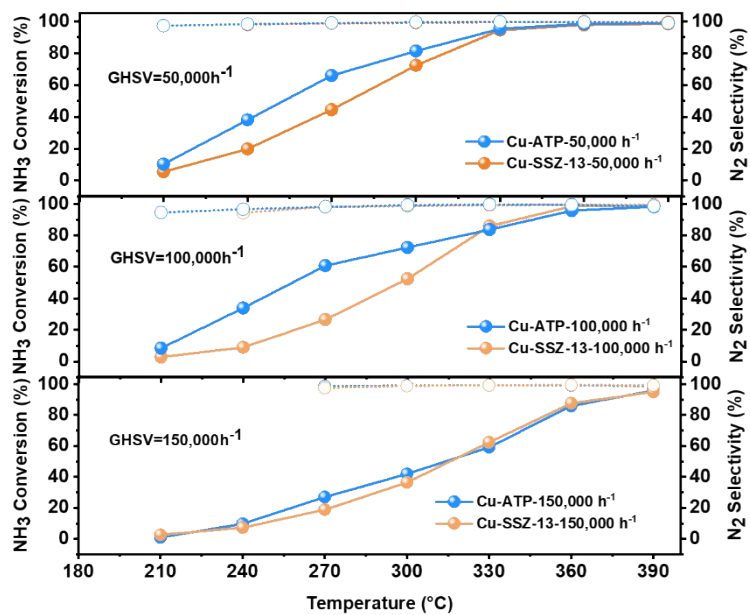


**Fig. S12.** Plots of NH<sub>3</sub> conversion (solid lines) and N<sub>2</sub> selectivity (dash lines) versus temperature over Cu-ATP and Cu-SSZ-13 catalysts. Reaction conditions: 500 ppm NH<sub>3</sub>, 5 vol % O<sub>2</sub> balanced with N<sub>2</sub>, and 50,000 h<sup>-1</sup>-150,000 h<sup>-1</sup> of GHSV.

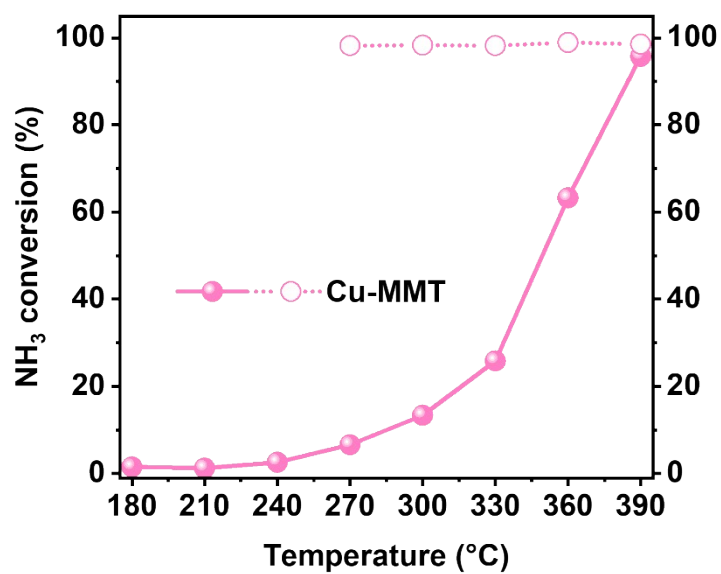


**Fig. S13.** Plots of NH<sub>3</sub> conversion (solid lines) and N<sub>2</sub> selectivity (dash lines) versus temperature over the Cu-MMT catalyst. Reaction conditions: 500 ppm NH<sub>3</sub>, 5 vol % O<sub>2</sub> balanced with N<sub>2</sub>, and 50,000 h<sup>-1</sup> of GHSV.

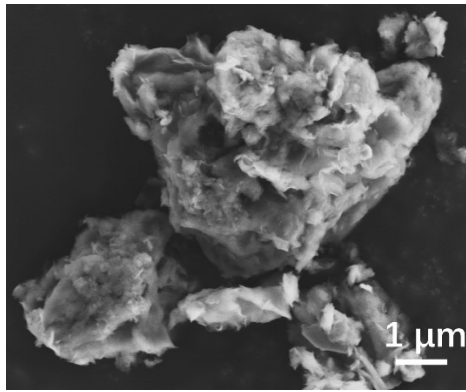


**Fig. S14.** SEM image of ATP support.

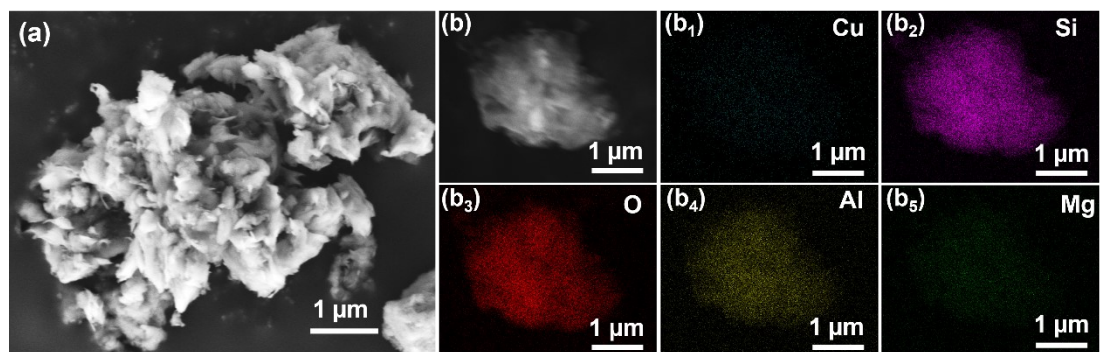


**Fig. S15.** (A) SEM image; (B) EDS mapping results of overlapped image and (B<sub>1</sub>) Cu, (B<sub>2</sub>) Si, (B<sub>3</sub>) O, (B<sub>4</sub>) Al, and (B<sub>5</sub>) Mg elements distribution over the Cu-ATP catalyst.

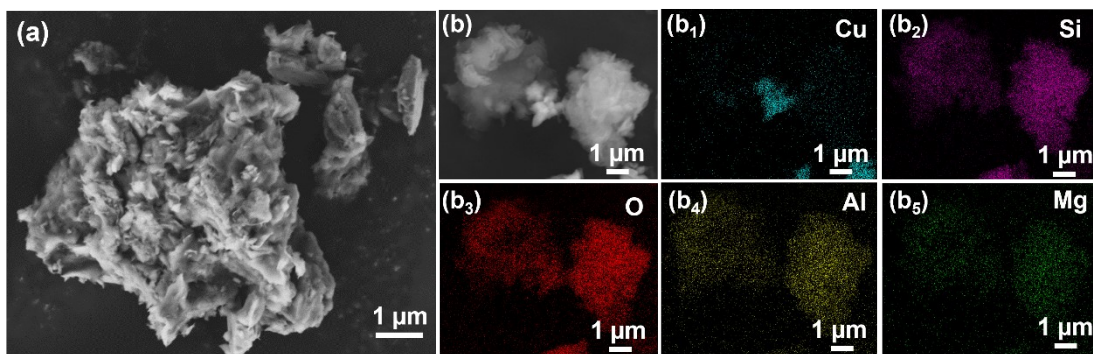


**Fig. S16.** (A) SEM image; (B) EDS mapping results of overlapped image and (B<sub>1</sub>) Cu, (B<sub>2</sub>) Si, (B<sub>3</sub>) O, (B<sub>4</sub>) Al, and (B<sub>5</sub>) Mg elements distribution over the CuO/ATP catalyst.

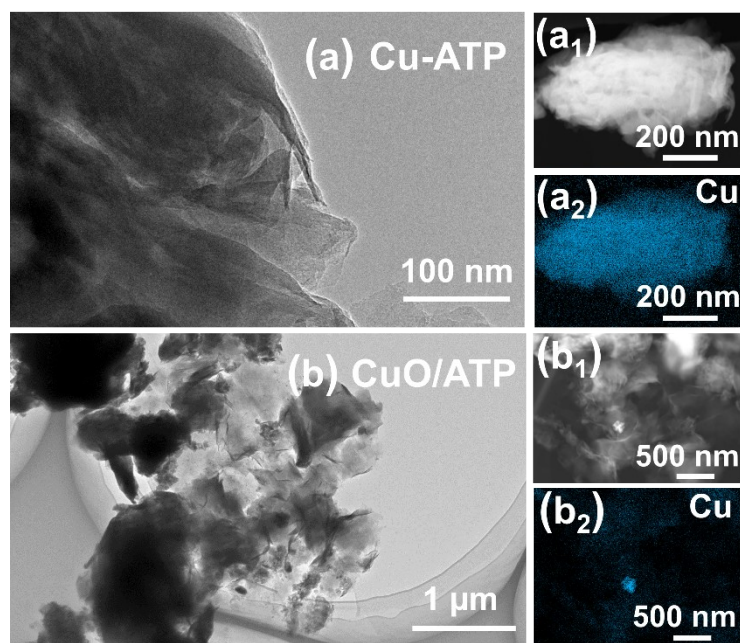


**Fig. S17.** (A) TEM image; (A<sub>1</sub>) EDS mapping results of overlapped image and (A<sub>2</sub>) Cu elements distribution over the Cu-ATP; (B) TEM image; (B<sub>1</sub>) EDS mapping results of overlapped image and (B<sub>2</sub>) Cu elements distribution over the CuO/ATP.

The ATP exhibited typical stacked rod-like morphology.<sup>1</sup> Moreover, the uniform dispersion of Cu species further demonstrated the possible presence of Cu<sup>2+</sup> or highly

dispersed Cu structure. But Cu elements existed as agglomerate particles in CuO/ATP.

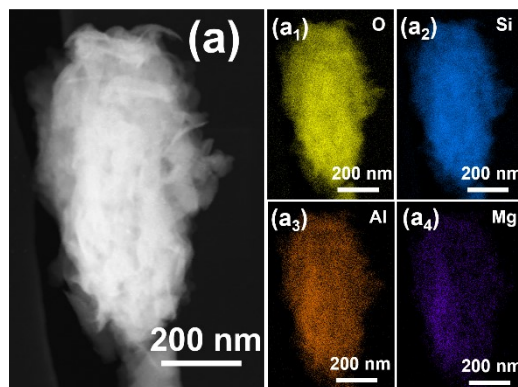


**Fig. S18.** (A) EDS mapping results of overlapped image and (A<sub>1</sub>) O, (A<sub>2</sub>) Si, (A<sub>3</sub>) Al, (A<sub>4</sub>) Mg elements distribution over the Cu-ATP catalyst.

The other skeleton elements such as Si、Al、O and small amount of Mg were evenly dispersed in the framework of the Cu-ATP catalyst.

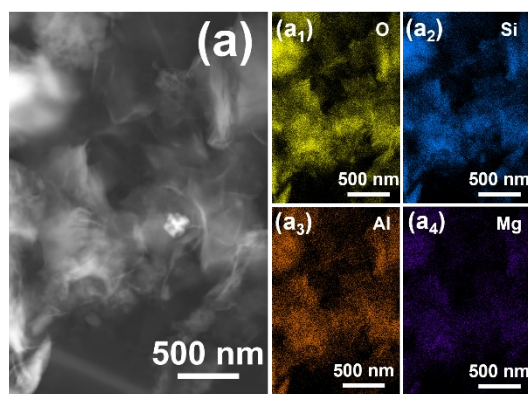


**Fig. S19.** (A) EDS mapping results of overlapped image and (A<sub>1</sub>) O, (A<sub>2</sub>) Si, (A<sub>3</sub>) Al, (A<sub>4</sub>) Mg elements distribution over the CuO/ATP catalyst.

Similarly, the skeleton elements on the CuO/ATP catalyst were also uniformly dispersed.

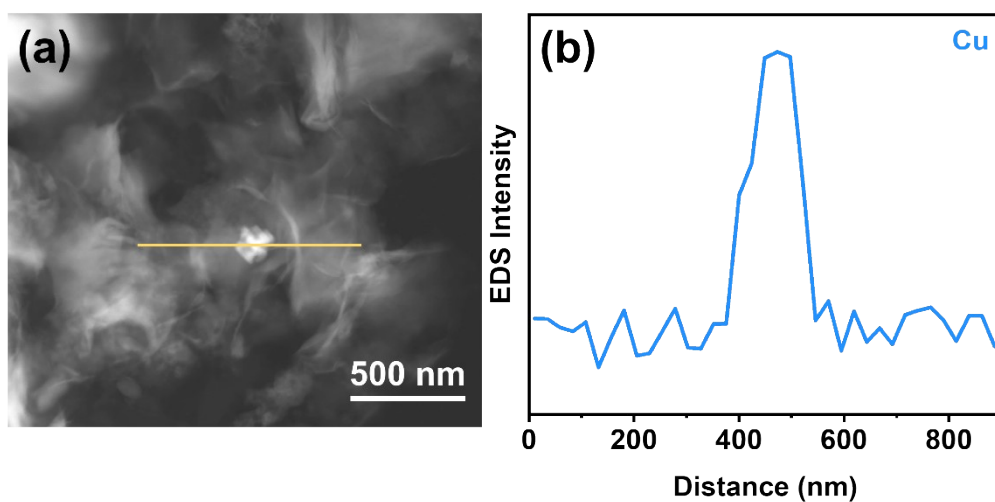


**Fig. S20.** The line scanning image of TEM-energy dispersive X-ray spectroscopy (EDS) over the CuO/ATP catalyst.

The CuO particles could be observed in TEM-EDS and the result of line scanning also proved the bright spot was related to Cu element.

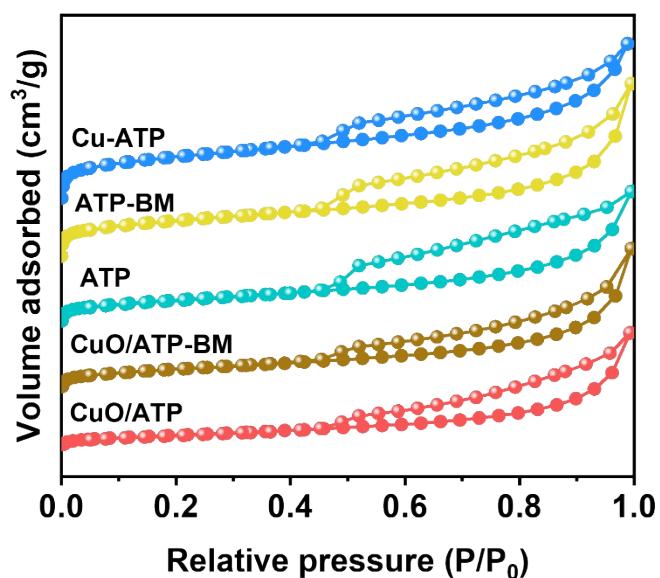


**Fig. S21.** N<sub>2</sub> physisorption isotherms of ATP support, ATP-BM, Cu-ATP, CuO/ATP and CuO/ATP-BM catalysts.

N<sub>2</sub> adsorption–desorption isotherms were measured for looking into the adsorption capacity to reactants over catalysts. The isotherm type was type IV, and it was H<sub>4</sub> hysteresis loop. The surface area of ATP support was 62.9 m<sup>2</sup>/g. Ball milling could increase the specific surface area to 89.2 m<sup>2</sup>/g. After Cu<sup>2+</sup> exchange, due to interlayer impurity removal, the further increase of specific surface area was beneficial to the adsorption of reactant molecules. On the contrary, the specific surface area decreased on account of the coating effect of CuO particles on the surface on CuO/ATP.

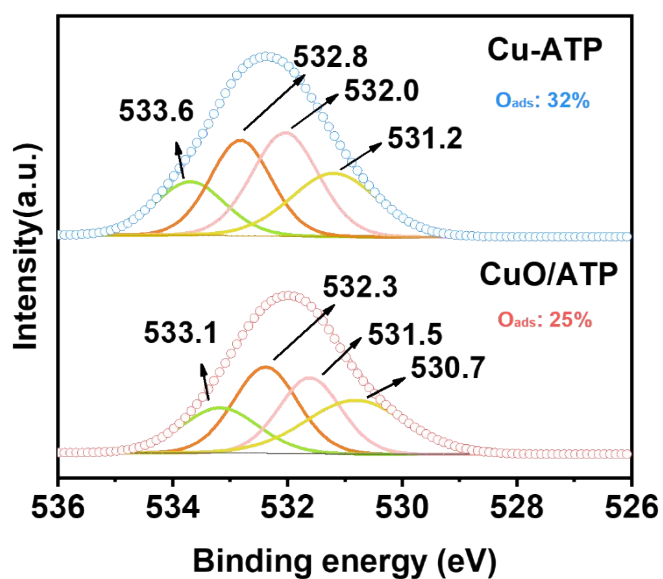


**Fig. S22.** O 1s XPS spectra for Cu-ATP and CuO/ATP catalysts.

In general, each spectrum could be fitted into four peaks, the binding energy peak around 530.7 eV assigned to the lattice oxygen ( $O_{\text{latt}}$ ), the binding energy peak around 531.5 eV assigned to the adsorbed oxygen ( $O_{\text{ads}}$ ) and the binding energy peak around 532.3 eV and 533.1 eV, likely to be associated with hydroxyl species and adsorbed water.<sup>2-4</sup>

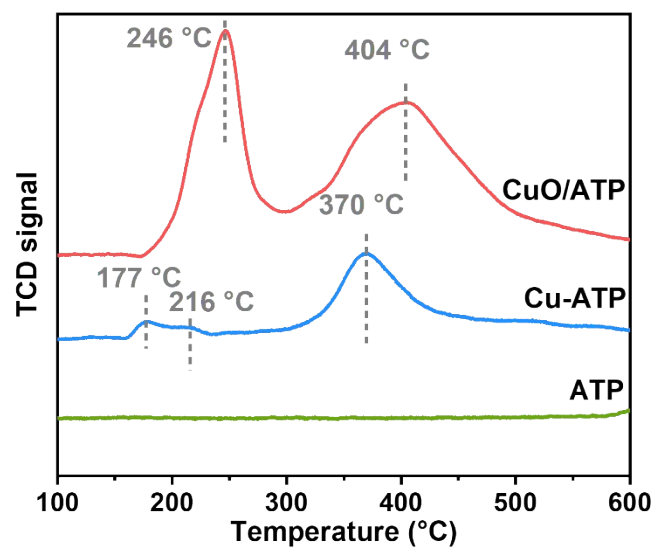


**Fig. S23.** H<sub>2</sub>-TPR profiles for Cu-ATP, CuO/ATP catalysts and ATP support.

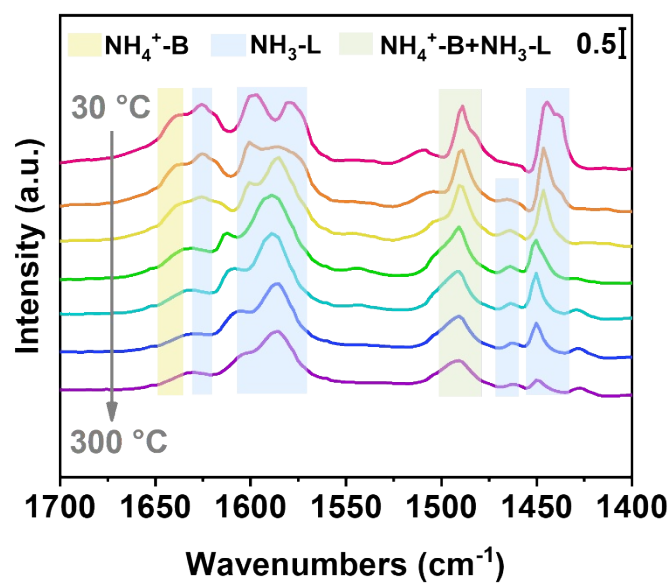


**Fig. S24.** Py-IR spectra for the Cu-ATP catalyst.

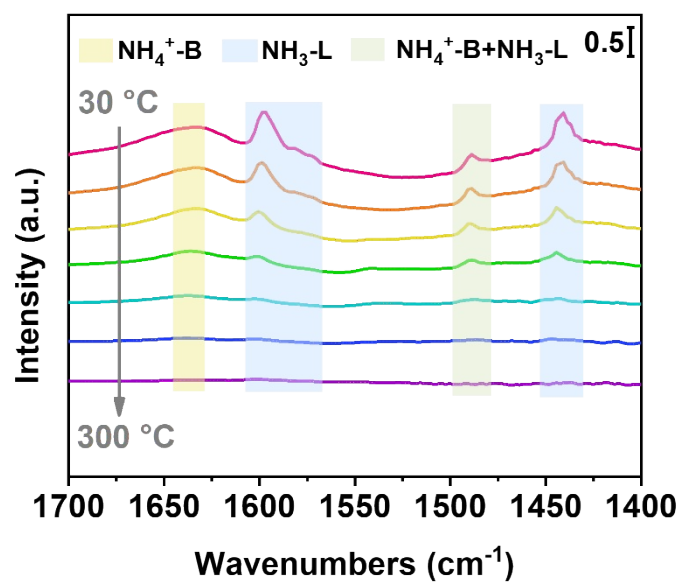


**Fig. S25.** Py-IR spectra for the CuO/ATP catalyst.

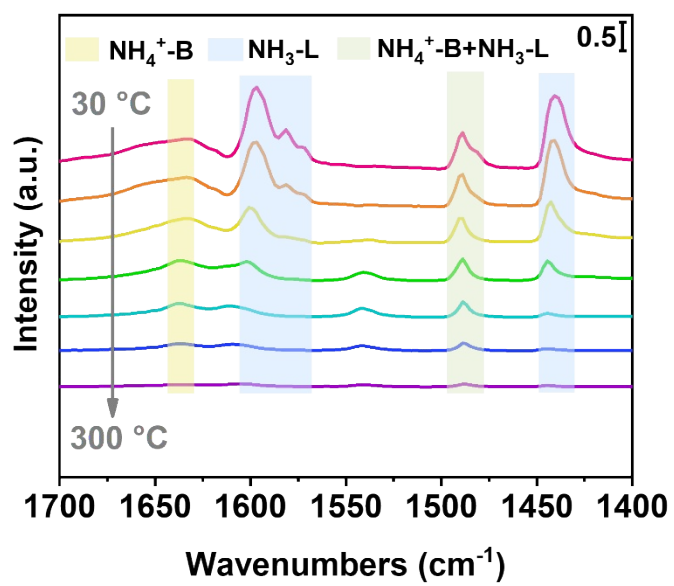


**Fig. S26.** Py-IR spectra for the ATP support.

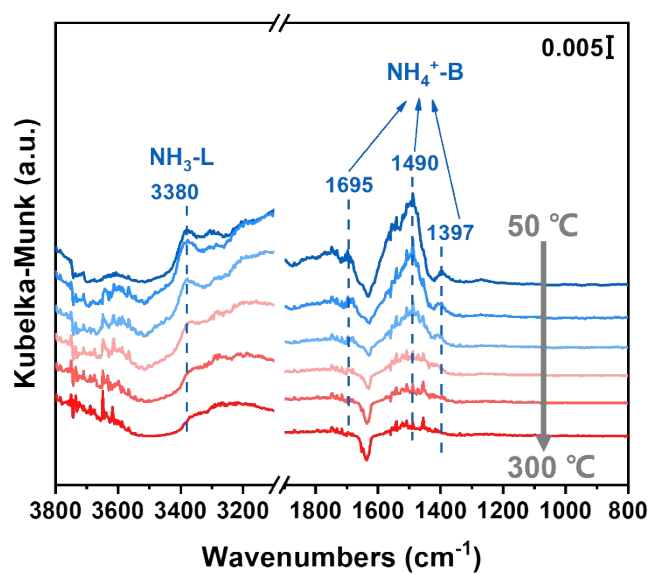


**Fig. S27.** The NH<sub>3</sub> adsorption spectra of ATP support.

On the ATP support, adsorption bands were observed at 1397, 1490 and 1695 cm<sup>-1</sup> might be the NH<sub>3</sub> adsorption at Brønsted acid sites.<sup>5, 6</sup> The band at 3380 cm<sup>-1</sup> was assigned to the NH<sub>3</sub> adsorption at Lewis acid site.<sup>7</sup>

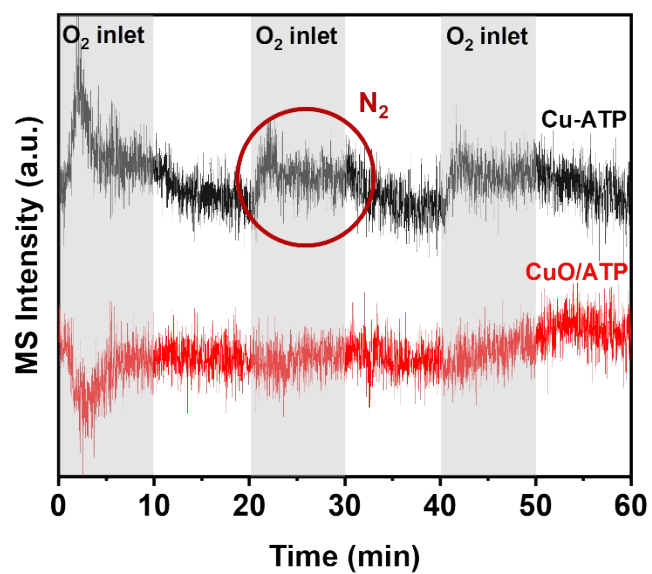


**Fig. S28.** The N<sub>2</sub> signal detected by mass spectrometry of Cu-ATP and CuO/ATP catalysts.

**Table S1.** Cu element content of Cu-ATP, CuO/ATP, Cu-SSZ-13, Cu-ZSM-5 and Cu-SAPO-34 catalysts.

| <b>Sample</b> | <b>Cu<br/>Content (wt%)</b> |
|---------------|-----------------------------|
| Cu-ATP        | 3.39                        |
| CuO/ATP       | 3.59                        |
| Cu-SSZ-13     | 2.83                        |
| Cu-ZSM-5      | 3.3                         |
| Cu-SAPO-34    | 3.15                        |

**Table S2.** The specific surface area, pore volume and pore size information obtained from the N<sub>2</sub> adsorption-desorption isotherms analysis of ATP support, ATP-BM, Cu-ATP, CuO/ATP and CuO/ATP-BM catalysts.

| <b>Sample</b> | <b>Surface Area (m<sup>2</sup>/g)</b> | <b>Pore Volume (cm<sup>3</sup>/g)</b> | <b>Pore Size (nm)</b> |
|---------------|---------------------------------------|---------------------------------------|-----------------------|
| ATP           | 62.9                                  | 0.11                                  | 10.2                  |
| ATP-BM        | 89.2                                  | 0.09                                  | 7.1                   |
| Cu-ATP        | 100.1                                 | 0.12                                  | 7.5                   |
| CuO/ATP-BM    | 56.1                                  | 0.08                                  | 8.0                   |
| CuO/ATP       | 34.5                                  | 0.10                                  | 13.5                  |

## References

1. Y. Zhao, L. Shi, Y. Shen, J. Zhou, Z. Jia, T. Yan, P. Wang and D. Zhang, Self-Defense Effects of Ti-Modified Attapulgite for Alkali-Resistant NO<sub>x</sub> Catalytic Reduction, *Environ. Sci. Technol.*, 2022, **56**, 4386-4395.
2. P. Venkataswamy, K. N. Rao, D. Jampaiah and B. M. Reddy, Nanostructured manganese doped ceria solid solutions for CO oxidation at lower temperatures, *Appl. Catal., B*, 2015, **162**, 122-132.
3. C. Zhang, C. Wang, W. Zhan, Y. Guo, Y. Guo, G. Lu, A. Baylet and A. Giroir-Fendler, Catalytic oxidation of vinyl chloride emission over LaMnO<sub>3</sub> and LaB<sub>0.2</sub>Mn<sub>0.8</sub>O<sub>3</sub> (B=Co, Ni, Fe) catalysts, *Appl. Catal., B*, 2013, **129**, 509-516.
4. X. Cao, W. Huo, M. Wang, H. Wei, Z. Lu and K. Li, Visible-light-assisted peroxydisulfate activation over Ag<sub>6</sub>Si<sub>2</sub>O<sub>7</sub>/Cu(II)-modified palygorskite composite for the effective degradation of organic pollutants by radical and nonradical pathways, *Environ. Res.*, 2022, **214**, 113970.
5. J. Wang, Z. Yan, L. Liu, Y. Chen, Z. Zhang and X. Wang, In situ DRIFTS investigation on the SCR of NO with NH<sub>3</sub> over V<sub>2</sub>O<sub>5</sub> catalyst supported by activated semi-coke, *Appl. Surf. Sci.*, 2014, **313**, 660-669.
6. L. Chen, Z. Si, X. Wu and D. Weng, DRIFT Study of CuO–CeO<sub>2</sub>–TiO<sub>2</sub> Mixed Oxides for NO<sub>x</sub> Reduction with NH<sub>3</sub> at Low Temperatures, *ACS Appl. Mater. Interfaces*, 2014, **6**, 8134-8145.
7. Z. Ma, X. Wu, H. Härelind, D. Weng, B. Wang and Z. Si, NH<sub>3</sub>-SCR reaction mechanisms of NbO<sub>x</sub>/Ce<sub>0.75</sub>Zr<sub>0.25</sub>O<sub>2</sub> catalyst: DRIFTS and kinetics studies, *J. Mol. Catal. A: Chem.*, 2016, **423**, 172-180.

